

# **Additive free co-deposition of nanocrystalline copper / cuprous oxide by electrodeposition**

**S.Y. Ng<sup>§</sup> and A.H.W. Ngan**

**Department of Mechanical Engineering,**

**The University of Hong Kong,**

**Pokfulam Road, Hong Kong, P.R. China**

**<sup>§</sup>Corresponding Author (Email: [angeln@hku.hk](mailto:angeln@hku.hk))**

## **Abstract**

We report a gradual transition in the deposition product from pure Cu<sub>2</sub>O to pure Cu, during electrodeposition on Au/Pd sputter-coated silicon wafer substrates in copper sulphate electrolyte with various dc potential. At voltages lower than 0.3V, only pure Cu in a nanocrystalline form is deposited on the cathode substrate, while at voltages higher than 1.2V, only pure Cu<sub>2</sub>O, also in a nano/microcrystalline form, is deposited. At intermediate voltages between 0.3 to 1.2 V, the deposition product comprises a mixture of both Cu and Cu<sub>2</sub>O nano/micro-crystals. The Cu<sub>2</sub>O crystals are generally of an octahedral shape with sizes ranging from 30nm to 100nm, while Cu nano/microcrystals are of irregular shape ranging from 100nm to 2μm. This work provides a method to fabricate nanocrystalline Cu<sub>2</sub>O, Cu and Cu/Cu<sub>2</sub>O on substrates in a single step without the use of additives.

**Keywords:** Cu/Cu<sub>2</sub>O co-deposition; cuprous oxide; Cu<sub>2</sub>O crystals; electrodeposition; nanocrystalline

## 1. Introduction

For many years, synthesizing and fabricating nanostructured materials have been of immense interest, since nano-scale materials often possess enhanced physical and chemical properties. Over the past decade, in addition to metals, nanostructured semiconductors and composites have attracted increasing attention. As a non-toxic semiconductor,  $\text{Cu}_2\text{O}$  nanostructures have been reported to exhibit Bose-Einstein condensation of excitons at lower light intensities [1].  $\text{Cu}_2\text{O}$  is also important in applications including solar cells [2], gas sensors [3] and photocatalysis in  $\text{H}_2$  production [4]. Metallic copper, on the other hand, has very different physical properties, the differentiation between the lattice parameters and the electrical resistivity of Cu and  $\text{Cu}_2\text{O}$  nanostructures can be used to produce rectifiers and resonant tunneling devices at room temperature [5].

Various techniques have been developed to synthesize different forms of  $\text{Cu}_2\text{O}$  nanostructures, such as thermal decomposition [6], thermal oxidation [7], dc sputtering [8], solution phase synthesis [9], and electrodeposition [10]. Of these, electrodeposition is regarded as an efficient and inexpensive method to fabricate nanostructures. Different compositions of the as deposited films can be controlled by varying the parameters of the electrochemical setup, and different nanostructures such as nanocrystals, nanowires, and nanocrystalline coatings of  $\text{Cu}_2\text{O}$ , have been fabricated by electrodeposition [11-13].

Co-deposition of Cu/Cu<sub>2</sub>O has also been reported to be favored only in high pH solution for electrodeposition, or with the use of different additives. Lee et. al. demonstrated that Cu/Cu<sub>2</sub>O composite nanowire arrays could be deposited by varying the pH value and potentials by using anodic aluminum oxide (AAO) [14]. Switzer et al. have fabricated Cu/Cu<sub>2</sub>O layered nanostructures by using Cu(II) lactate and in alkaline solution [15]. Luo et. al. have fabricated copper nanocubes and Cu<sub>2</sub>O depositions and studied the effect of temperature, pH value and reaction time on the shape evolution [16]. All of these studies made use of alkaline media. Yu et al showed that Cu/Cu<sub>2</sub>O fingering branches of deposits can be obtained without changing the pH value, but a complicated setup and an ultrathin layer of electrolyte are needed [17].

We have recently used electrodeposition to fabricate Cu<sub>2</sub>O nanocrystals and nanowires on different substrates such as Si wafer, stainless steel plate and HOPG [11, 12], by cathodic reactions. In the present study, we report an additive-free electrodeposition approach to co-deposit nanocrystalline Cu/Cu<sub>2</sub>O at room temperature.

## **2. Experimental methods**

The electrolyte was prepared by mixing analytical-grade copper (II) sulphate (supplied by Sigma Aldrich Co Ltd.) and distilled water to achieve a concentration of 0.018M. The electrolyte was ultrasonically treated for 10 min before the experiments to ensure good solubility. The pH value was measured to be 4.0. A simple two-electrode system was used for the experiments.

1” diameter x 250 $\mu$ m thickness [100]-oriented silicon wafers (supplied by Universitywafer.com) were used as the substrates. Before electrodeposition, the Si wafers were sputtered with Au/Pd for 220s at 15 $\mu$ A by using a sputter coater (BAL-TEC SCD 005). During electrodeposition, the silicon substrate was used as the cathode while a 0.5mm x 30mm x 50mm polished copper plate (with purity > 99.9%) was used as the anode. Deposition potentials were controlled by an electrochemical workstation (LK2006A, Lanlike). The electrodes were separated by a distance of 20mm, and the whole electrodeposition process was kept at room temperature. All experiments were carried out under constant voltage conditions. After electrodeposition, the substrates were rinsed several times with distilled water and ethanol, and were put inside a desiccator at room temperature before characterization. A set of experiments was conducted by varying the deposition potential from 0.3V to 1.2V in order to study the effect of the deposition potential on the volume fraction of the Cu content in the co-deposition process.

The morphology and chemical composition were characterized by a field-emission scanning electron microscope (FEG SEM, Hitachi S4800) equipped with energy-dispersive x-ray spectroscopy (EDX) analysis function, x-ray diffraction (XRD, Bruker D8 diffractometer) equipped with a Cu X-ray tube operated at 40kV and 30mA and a transmission electron microscope (scanning TEM, FEI Tecnai G2 20) operating at 200kV.

### 3. Results

#### 3.1. Co-deposition of nanocrystalline Cu/Cu<sub>2</sub>O

Fig. 1(a) is an SEM image of the co-deposition of Cu<sub>2</sub>O and Cu crystals on a Si substrate using a voltage of 0.5V for 60s. Two types of crystals were formed on the substrate: first, Cu<sub>2</sub>O nanocrystals of octahedral shape in general which were quite uniformly distributed over the substrate surface, and secondly, larger Cu nanocrystals of irregular shapes. The edge length of the Cu<sub>2</sub>O nanocrystals ranged from 30nm to 100nm. In terms of shape, about 82% of Cu<sub>2</sub>O crystals were perfectly octahedral, the rest of them were truncated octahedrons. On the other hand, the diameter of the Cu crystals ranged from 100nm to 500nm. Fig. 1(b) shows an SEM image of the co-deposition at 0.5V for 600s. Compared with Fig. 1(a), the size of both the Cu<sub>2</sub>O and Cu crystals increased with the increased deposition time. It can be seen that small nanocrystals were deposited on the surface of the larger Cu crystals. These deposited nanocrystals were not randomly distributed on the surface of the Cu crystals, but were more preferentially deposited on their edges. As shown in the mapping analysis in Fig. 3, O is found on the surface of the Cu crystals, suggesting that these nanocrystals were Cu<sub>2</sub>O. It is believed that since the Cu crystals contained surface protrusions, they intensified the electric field and favour further growth. The electric field around the edges of the Cu crystals was particularly high, and when Cu<sup>2+</sup> ions reached there, they became reduced and form Cu<sub>2</sub>O nanocrystals on the edges, and continued deposition led to preferential deposition on the edges as shown in Fig. 1(b).

The two types of crystals in Fig. 1 were identified by electron diffraction as well

as by compositional analysis. Fig. 2 shows a TEM bright-field image of several nano/micro-crystals desquamated from a Si substrate. The upper selected-area electron diffraction (SAED) pattern was taken along the [112] zone of a typical octahedral Cu<sub>2</sub>O nanocrystal at position (i) marked. The {110} and {111} reflections are indicated in the diffraction pattern. The nanocrystal shows a cubic structure with a lattice constant of  $0.42 \pm 0.01$  nm which is in agreement with the known value of 0.427 nm for Cu<sub>2</sub>O [18]. The lower SAED pattern was taken along the  $[01\bar{1}]$  zone of a larger microcrystal at position (ii). The {111} and {200} reflections are indicated in the diffraction pattern, and the lattice constant was calculated to be  $0.36 \pm 0.01$  nm, which is in agreement with the value of 0.362 nm for Cu [19].

To confirm the chemical compositions of the deposited products, EDX point analysis and mapping were performed. Fig. 3 shows the EDX composition spectroscopy and mapping of the deposited products at 0.5V for 600s. The point analysis results in the right panel of Fig. 3 show that only Cu was present in the large micro-crystal labeled as (iii), while both Cu and O were detected at the octahedral nanocrystals labeled as (iv). Moreover, in the mapping analysis, it can be seen that Cu is intensively detected at the two larger particles, but O is uniformly distributed all over the substrate area, suggesting that the two larger particles are copper microcrystals. Oxygen is also detected on the surface of the two Cu micro-crystals, indicating that the surface of the Cu has been slightly oxidized.

### **3.2 Pure nanocrystalline Cu<sub>2</sub>O deposition**

At a lower electrodeposition potential, pure  $\text{Cu}_2\text{O}$  nanocrystals were obtained. Fig. 4(a) shows a low-magnification SEM image of the deposited  $\text{Cu}_2\text{O}$  nanocrystals deposited at 0.1V for 60s on a Si substrate. As shown in the example in the inset of Fig. 4(a), the deposited crystals typically exhibit an octahedral shape with edge length of 100nm. To reconfirm the structure of all the as-synthesized nanocrystals, large quantities of nanocrystals were desquamated from the substrate and studied by TEM with a selected-area aperture large enough to cover many nanocrystals. Fig. 4(b) shows a resultant SAED pattern comprising dotted concentric rings, all of which can be identified to belong to the simple cubic structure of  $\text{Cu}_2\text{O}$ .

### **3.3 Pure nanocrystalline Cu deposition**

At a higher potential, pure Cu nanocrystals were obtained. Fig. 5 shows an SEM image of the deposited Cu microcrystals deposited at 1.2V for 60s on a Si substrate. As can be seen in the image, no octahedral nanocrystals were present, and the whole area was covered by irregular shaped Cu nanocrystals. To characterize the structure of the deposited nanocrystals, EDX spectroscopy was performed. The results of EDX (not shown) show that only Cu was detected which supports the product crystals to be copper.

Fig. 6 is the XRD patterns of the deposited products obtained at different deposition potentials. All of the diffraction peaks are indexed according to the standard cubic structures of copper (JCPDS file No. 85-1326) and the standard diffraction peaks of cuprous oxide (JCPDS file No. 78-2076). The nanocrystals

deposited at 0.3V were pure Cu<sub>2</sub>O as shown in Fig. 6(a). The results indicate that only Cu<sub>2</sub>O is present on the deposited product. The peaks are attributed to the {111} and {220} reflections of Cu<sub>2</sub>O and those from the Si substrate (marked with solid stars). As a deposition potential of 0.7V, Cu reflections emerge as indicated by solid square symbols in Fig. 6(b). The results indicated that both Cu and Cu<sub>2</sub>O co-existed on the deposition products. Besides the reflections of Cu<sub>2</sub>O, the diffraction peaks at  $2\theta = 43.8^\circ$ ,  $50.9^\circ$  and  $74.4^\circ$  correspond to the {111}, {200} and {220} reflections of the cubic Cu. It can be seen that initially, Cu<sub>2</sub>O(220) is dominant but then Cu<sub>2</sub>O(111) becomes stronger as the potential increases before both peaks disappear at high potential. This is thought to be due to the fact that at a lower potential, the deposited Cu<sub>2</sub>O nanocrystals are mostly truncated octahedrons, but at a higher potential, more Cu<sub>2</sub>O nanocrystals grew into octahedrons each consisting of eight (111) planes, so that the intensity of Cu<sub>2</sub>O(111) becomes stronger as the potential increased. As the applied potential is increased to 1.2V, the reflections of Cu<sub>2</sub>O disappeared, and only those of Cu remained as shown in Fig. 6(c).

### **3.4 Effects of electrodeposition potentials on volume fractions of Cu content**

By controlling the electrodeposition potential, different products can be obtained. Pure Cu<sub>2</sub>O nanocrystals were obtained at potentials below 0.3V, while pure Cu nanocrystals were obtained for potentials higher than 1.2V. From 0.3V to 1.2V, both Cu and Cu<sub>2</sub>O were found as Cu/Cu<sub>2</sub>O co-deposition. The relative fraction of the co-deposition product can be controlled by varying the applied potential.

Fig. 7 shows the volume fraction of Cu in the deposition product at different deposition potentials on Si wafer substrates. The deposition duration for all the experiments was maintained at 60s. The insets are representative SEM micrographs showing the distributions of the Cu and Cu<sub>2</sub>O nanocrystals at different deposition potentials. It can be seen that as the potential was increased from 0.5V to 1.2V, the volume percentage of Cu content increased from 65% to 97%. Insets B to D show the distribution of Cu and Cu<sub>2</sub>O nanocrystals deposited on Si at the corresponding potentials. Below 0.3V, the deposition product was pure Cu<sub>2</sub>O as mentioned before, and the substrate was fully covered by octahedral Cu<sub>2</sub>O nanocrystals as shown in inset A. Above 1.2V, the deposition product became pure Cu with no Cu<sub>2</sub>O nanocrystal found, and the substrate was fully covered by irregular shaped Cu nanocrystals as shown in inset E. It is, however, important to note that the experiments here were performed using a two-electrode set-up, and so the true cathode potential was not fixed. The current values measured at the applied potential of 0.3V, 0.5V and 1.2V were ~1mA, ~3.3mA and ~9mA respectively, at which Cu<sub>2</sub>O, Cu/Cu<sub>2</sub>O and Cu were electrodeposited. It is clear that deposition of pure Cu<sub>2</sub>O only needed a small current, while larger current was needed for the deposition of Cu.

As for the size of the crystals, the edge length of the Cu<sub>2</sub>O crystals did not change much but the average size of the Cu crystals decreased as the deposition potential increased. At potential 0.3V, the edge length of Cu<sub>2</sub>O is 63nm which is similar to that at 0.9V, while for Cu crystal, it is 300nm at 0.5V compared to 200nm at 1.2V.

#### 4. Discussion

In the present experiments, the micro- and nano-crystals formed on the Si wafer substrates were identified to be Cu and Cu<sub>2</sub>O depending on the potential used. The Cu<sub>2</sub>O crystals were also found to have an octahedral shape in the steady state. In the literature, Cu<sub>2</sub>O nanocrystals and co-deposition of Cu and Cu<sub>2</sub>O were usually obtained by electrodeposition in alkaline media [15] or with the use of additives in the electrolyte [16]. In this study, however, we successfully fabricated nanosized single crystals of Cu<sub>2</sub>O, co-deposition of Cu and Cu<sub>2</sub>O, as well as pure Cu nanocrystals, on Si wafer by low-potential electrodeposition using a simple two-electrode setup at room temperature (25°C) at pH 4. Comparing to the study by Switzer et. al. [15], the Cu content at a given current density is a strong function of the solution pH, namely, as the pH increased, the Cu content decreased. At pH 12, the films deposited were pure Cu<sub>2</sub>O even for relatively high current densities. However, in the present study, the electrolyte pH was maintained constant, and so the variation of the Cu fraction is all accounted for by the deposition potential.

The cyclic voltammogram of copper sulfate is known to exhibit two reductive peaks [16], which indicate that the electrochemical reduction of Cu(II) ions proceeds via two steps, namely, (i) the reduction of Cu(II) ions to Cu(I) ions, and (ii) the further reduction of Cu(I) ions to form Cu metal. Since both Cu<sub>2</sub>O and Cu can be deposited according to the present experiments, the possible chemical reactions at the cathode that correspond to the two-step reduction of Cu(II) are as follows:

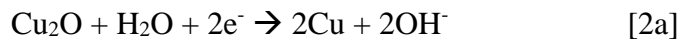
(i) First reduction step Cu(II) → Cu(I)



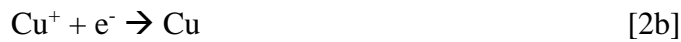
or



(ii) Second reduction step Cu(I) → Cu



or



The results in Fig. 7 may then be explained on the basis of such a two-step reduction process of Cu(II). Below ~0.3V, the cathode over-potential is sufficient to enable the first reduction step to occur, so that Cu(II) ions would reduce to form Cu<sub>2</sub>O according to Eq. [1a], but the potential is not high enough to allow the further reduction of Cu(I) in Eq. [2a] to proceed. Therefore, only Cu<sub>2</sub>O results in the reaction product. The absence of Cu in the deposition product in this potential range also suggests that Eqs. [1b] and [2b] are not operative in this regime. This is supported by the fact that the equilibrium electrode potential of Cu<sub>2</sub>O (0.347V) vs standard hydrogen electrode is higher than that of Cu (0.297V) [17], which indicates that the cathodic formation of Cu<sub>2</sub>O is thermodynamically more favorable than Cu in CuSO<sub>4</sub> electrolyte at low over-potentials.

At higher potentials in the range between  $\sim 0.3\text{V}$  and  $\sim 1.2\text{V}$ , the cathode over-potential is large enough to allow both reduction steps of  $\text{Cu(II)}$  to occur, so that both  $\text{Cu}_2\text{O}$  and  $\text{Cu}$  are deposited on the substrate (Fig. 7). Nucleation of  $\text{Cu}_2\text{O}$  may first occur on the substrate according to Eq. [1a], and some of the  $\text{Cu}_2\text{O}$  seeds may be further reduced to form  $\text{Cu}$  nanocrystals according to Eq. [2a]. Alternatively, Eqs. [1b] and [2b] may become operative in this potential regime, so that  $\text{Cu(II)}$  ions arriving from the electrolyte may directly form  $\text{Cu}$  nanocrystals on the substrate without undergoing the  $\text{Cu}_2\text{O}$  formation as an intermediate step. Once  $\text{Cu}$  seeds are formed on the substrate surface from either alternative route, they act as concentrators of electric field on the substrate surface since their counterpart,  $\text{Cu}_2\text{O}$ , is a semi-conductor with a much lower electrical conductivity. Fresh  $\text{Cu(II)}$  ions from the electrolyte are thus preferentially attracted to the surface of the  $\text{Cu}$  nanocrystal seeds and get reduced on them according to Eqs. [1b] and [2b]. As the  $\text{Cu}$  crystals become larger than the  $\text{Cu}_2\text{O}$ , they become surface protrusions which further intensify the electric field, thus further enhancing their growth compared with that of the  $\text{Cu}_2\text{O}$ . This explains the present observation in Figs. 1 and 7 that the  $\text{Cu}$  crystals were much larger than the  $\text{Cu}_2\text{O}$  at the same deposition time. On the other hand, our previous study has shown that even in the regime where only  $\text{Cu}_2\text{O}$  is deposited, the crystal size of  $\text{Cu}_2\text{O}$  did not change significantly as the deposition time or potential increased [11], and inspection of Fig. 7 here shows that the crystal size of  $\text{Cu}_2\text{O}$  also did not change significantly with the deposition potential in the  $\sim 0.3$  to  $1.2\text{V}$  regime where  $\text{Cu}_2\text{O}$  and  $\text{Cu}$  were co-deposited. As discussed previously [11], this is attributed to a competition between crystal

nucleation and growth. At low deposition potentials, the ion flux arriving at the electrode from the electrolyte is low and the ions may have enough time to diffuse to favorable sites for nucleation, so that the Cu<sub>2</sub>O nuclei may grow slowly with a limited crystal size observed. At higher potentials, the ion flux is large and so many nuclei may form simultaneously on the substrate. The further arriving ion flux is therefore shared by a high density of nuclei, and so the growth of each Cu<sub>2</sub>O nucleus is also slow.

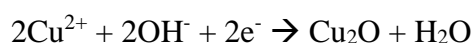
As the potential increases beyond ~0.3V, the rate of the Cu(I) → Cu reduction step increases, and so the Cu content increases with potential as shown in Fig. 7. Eventually, at potentials above ~1.2V, only Cu is observed to form which suggests that any Cu<sub>2</sub>O produced by Eq. [1a] is further reduced to form Cu via Eq. [2a]; the overall reaction is thus effectively



In this regime, the arriving Cu(II) ion flux is utilized mostly in forming new nuclei of Cu rather than supporting the growth of existing ones. As the ion flux is shared by more nuclei, the size of the Cu crystals becomes smaller at higher potentials.

Under the additive free condition, Cu<sup>2+</sup> ions undergo Eq. [1a]. They react with water and are reduced to form Cu(I) oxide on the cathode, releasing H<sup>+</sup> to the solution. The possible mechanism of Cu<sub>2</sub>O can be described as follows. First, during electrodeposition, the Cu<sup>2+</sup> ions were driven by electric field to the cathode. As mentioned, the equilibrium electrode potential of Cu<sub>2</sub>O is relatively high, and so it is deposited with priority. At a low deposition voltage, Cu<sup>2+</sup> ions are slowly attracted to

the surface of the cathode, and they have time to find thermodynamically favorable locations to attach to and get reduced to form flat and smooth surfaces with the lowest specific energy, {111} planes. The mechanism here described is different from that reported by Switzer et al [15] and Luo et al [16] who investigated the deposition of Cu/Cu<sub>2</sub>O by using alkaline medium and by using additive sodium dodecyl sulphate (SDS) respectively. The chemical reaction under alkaline medium is as follows:



Additive works by preferentially adsorbing on {111} planes, blocking other ions from the electrolyte approaching those faces and hindering the growth along <111> directions, and therefore octahedral-shaped crystals are formed. In this study, we managed to fabricate Cu<sub>2</sub>O without using additive and changing the pH of the solution.

## 5. Conclusions

We reported a facile method to achieve co-deposition of nanocrystalline Cu/Cu<sub>2</sub>O, and deposition of pure Cu and pure Cu<sub>2</sub>O nanocrystals, by electrochemical deposition. For potentials higher than 1.2V, the deposition product was pure Cu while for potentials lower than 0.3V, the deposition product was pure Cu<sub>2</sub>O. Also, without the use of any additives or changing the pH value of the electrolyte, different volume fractions of co-deposited Cu and Cu<sub>2</sub>O can be obtained by simply controlling the

deposition potential. The growth mechanisms of the deposited products and the effect of the deposition potential on the size of the  $\text{Cu}_2\text{O}$  and Cu crystals have also been discussed.

### **Acknowledgments**

This work is supported by funding from Kingboard Endowed Professorship in Materials Engineering. We are also grateful to Prof. K.Y. Chan for useful discussions.

## Figure Captions

Fig. 1. SEM image showing (a) the distribution of Cu/Cu<sub>2</sub>O nanocrystals electrodeposited over Si substrate at 0.5V for 60s, (b) co-deposition of Cu<sub>2</sub>O nanocrystals and Cu microcrystals at 0.5V for 600s.

Fig. 2. TEM bright-field image of Cu<sub>2</sub>O nanocrystals and Cu microcrystals deposited on Si substrate. Upper: Selected-area electron diffraction (SAED) pattern of the as-deposited Cu<sub>2</sub>O nanocrystal at zone [112] at position (i). Lower: SAED pattern of the as-deposited Cu microcrystal at zone [01 $\bar{1}$ ] at position (ii).

Fig. 3. EDX composition spectroscopy at positions (iii) and (iv), and mapping spectroscopy of the deposited products at 0.5V for 600s.

Fig. 4. (a) SEM image showing Cu<sub>2</sub>O nanocrystals deposited on a Si substrate at 0.1V for 60s. The inset shows a single octahedral shaped Cu<sub>2</sub>O nanocrystal in high magnification. (b) SAED pattern of Cu<sub>2</sub>O nanocrystals desquamated from Si substrate.

Fig. 5. SEM image showing the distribution of Cu nanocrystals deposited over a Si substrate at 1.2V for 60s.

Fig. 6. The XRD patterns of the nanocrystals obtained at different deposition potentials: (a) 0.3V, (b) 0.7V and (c) 1.2V.

Fig. 7. Percentage volume fraction of Cu at different deposition potentials on Si wafer substrates.

## References

1. D. Snoke, *SCIENCE-NEW YORK THEN WASHINGTON-*, 1351 (1996).
2. A. Mittiga, E. Salza, F. Sarto, M. Tucci and R. Vasanthi, *Applied Physics Letters*, **88**, 163502 (2006).
3. S. Deng, V. Tjoa, H. M. Fan, H. R. Tan, D. C. Sayle, M. Olivo, S. Mhaisalkar, J. Wei and C. H. Sow, *Journal of the American Chemical Society*, **134**, 4905 (2012).
4. D. Barreca, P. Fornasiero, A. Gasparotto, V. Gombac, C. Maccato, T. Montini and E. Tondello, *ChemSusChem*, **2**, 230 (2009).
5. J. A. Switzer, C.-J. Hung, L.-Y. Huang, E. R. Switzer, D. R. Kammler, T. D. Golden and E. W. Bohannon, *Journal of the American Chemical Society*, **120**, 3530 (1998).
6. M. Salavati-Niasari and F. Davar, *Materials Letters*, **63**, 441 (2009).
7. A. Musa, T. Akomolafe and M. Carter, *Solar Energy Materials and Solar Cells*, **51**, 305 (1998).
8. A. S. Reddy, S. Uthanna and P. S. Reddy, *Applied surface science*, **253**, 5287 (2007).
9. L. Gou and C. J. Murphy, *Nano Letters*, **3**, 231 (2003).
10. Y. Mao, J. He, X. Sun, W. Li, X. Lu, J. Gan, Z. Liu, L. Gong, J. Chen and P. Liu, *Electrochimica Acta*, **62**, 1 (2012).
11. S. Ng and A. Ngan, *Electrochimica Acta*, **56**, 7686 (2011).

12. S. Ng and A. Ngan, *Electrochimica Acta*, **114**, 379 (2013).
13. Y. Tang, Z. Chen, Z. Jia, L. Zhang and J. Li, *Materials letters*, **59**, 434 (2005).
14. Y.-H. Lee, I.-C. Leu, M.-T. Wu, J.-H. Yen and K.-Z. Fung, *Journal of alloys and compounds*, **427**, 213 (2007).
15. J. A. Switzer, C.-J. Hung, L.-Y. Huang, F. S. Miller, Y. Zhou, E. R. Raub, M. G. Shumsky and E. W. Bohannon, *Journal of materials research*, **13**, 909 (1998).
16. B. Luo, X. Li, X. Li, L. Xue, S. Li and X. Li, *CrystEngComm*, **15**, 5654 (2013).
17. G. Yu, X. Hu, D. Liu, D. Sun, J. Li, H. Zhang, H. Liu and J. Wang, *Journal of Electroanalytical Chemistry*, **638**, 225 (2010).
18. JCPDS File No. 78-2076
19. JCPDS File No. 85-1326